University of Groningen

Bachelor Thesis

Scanning and Locking an Optical Resonator

Author:
Tanay Veeragandham

Supervisors:
Steven Hoekstra
Jelle Aalbers

January 28, 2025

Abstract

The aim of this experiment is to scan and characterize an optical cavity, composed of highly reflective mirrors to amplify light intensity and create regions of high optical power that are ideal for trapping and studying nanoparticles. By characterizing the cavity and locking its resonance to maximize performance, this work establishes the foundation for experiments in nanoparticle trapping. Key characteristics such as finesse and power build up factor can be used to define the stability of the setup. The finesse of the cavity was experimentally found to be 557 ± 119 indicating a well-aligned cavity with mirrors with high reflection coefficients. The reflectivity of the mirrors was found to be $(99.32 - 99.56)\%$ while the power build up factor inside the cavity was 177.3 ± 37. The second part of the experiment involved locking the cavity to the side of a TEM_{00} peak, which is known as Side-of-Fringe locking, using an autolocking system. The deviation of the transmitted light signal was 4.6% from the mean. It was also observed that the system was being influenced by external environmental factors which exhibits the sensitive nature of the lock. Future efforts will focus on implementing Pound-Drever-Hall locking to enhance stability and enable multi-particle trapping experiments.

Contents

1 Introduction

In the late 19th century it has been theorized that light carries momentum which can be transferred to a particle by Maxwell and Bartoli. Experimental evidence of this was provided by Lebedev [1] and also by Nichols and Hull [2]. However for the radiation force to have an experimentally meaningful magnitude a laser had to be used which arrived in the late 1960s [3]. In 1970, Arthur Ashkin became the first to observe the acceleration of freely suspended microparticles by using radiation force. The experiments included using transparent latex spheres of $0.59, 1.31$ and $2.68 \mu m$ diameters suspended in water. A TEM_{00} mode beam of an argon laser was used for the radiation pressure. Realizing the nature of radiation pressure on microparticles, Ashkin went on to construct a true optical potential well with two opposing equal TEM_{00} Gaussian beams as shown in figure 1.

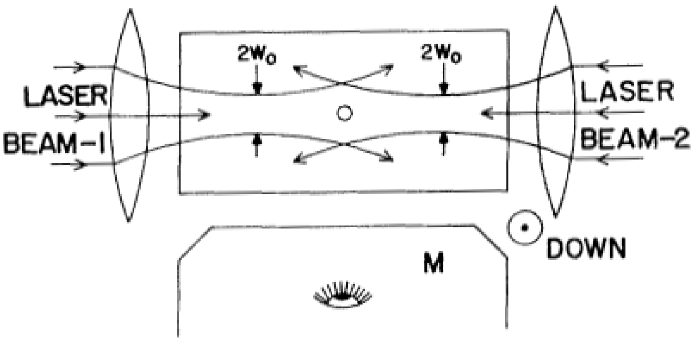

Figure 1: *Illustration of the concept of an optical well created by two counter-propagating laser beams. This standing wave generates alternating high and low intensity regions (antinodes and nodes), resulting in an optical lattice [4].*

This thesis aims to step in the direction of bridging the hazy gap between the quantum and the classical world. Nanospheres having numerous practical applications such as in the biophysics, mechanical engineering and even in observing quantum gravity due to their particle size, large surface area, and great biocompatibility. Silica Nanoparticles (SiNPs) which are composed of silicon dioxide with radius of 100 nm - 200 nm are used [5]. Silica is chosen as it is inert in most environments and is transparent to the electromagnetic radiation from most of the visible light spectrum [6].

The integration of optical cavities in trapping added another layer of precision and stability. In traditional optical tweezers a tightly focused beam generates sufficient force to trap small particles. Sometimes these setups are limited by the intensity and spatial distribution of the beam. However in this experiment, the use of a cavity overcomes this by amplifying the field and creating stable trapping regions by reducing scattering effects.

Cavity scanning is a crucial step in the trapping of nanoparticles since alignment is a critical prerequisite for characterizing the resonance modes. This experiment aims to find out the optimal conditions required to stabilize a cavity suitable for nanoparticle trapping by determining key characteristics such as finesse and power build factor.

2 Theory

2.1 Trapping Nanoparticles

This experiment involves only scanning and locking an optical cavity, however it serves as a base for future trapping setups. Optical cavities enhance the efficiency of trapping by amplifying the intensity of the laser beam, thereby increasing the gradient force.

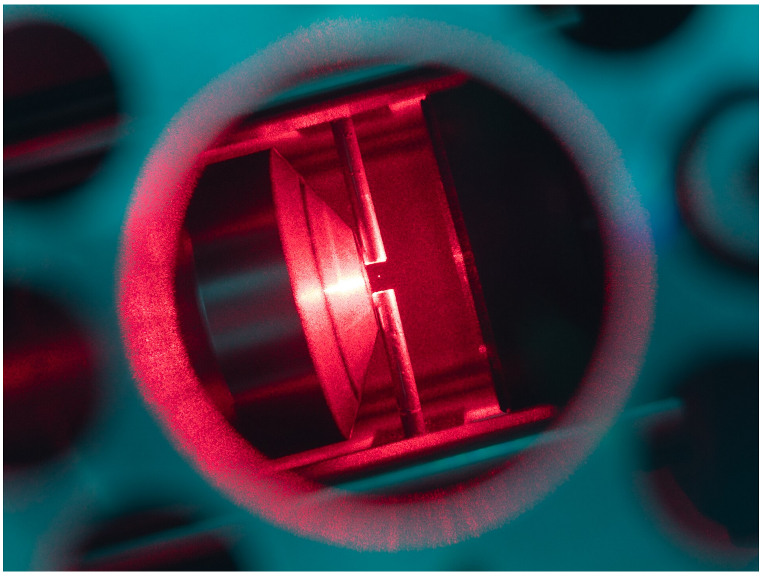

Figure 2: *A nanosphere trapped using an optical tweezer surrounded by electrodes to study the mass and shape distributions. [7].*

Trapping relies on forces exterted by highly focused laser beams to confine these dielectric nanospheres. These forces are explained in 2.4. Figure 2 shows a silica nanosphere trapped in an optical tweezer in a controlled pressure environment. The setup consisted of copper electrodes which were used to charge the particle. Part of the transmitted light was collected by a lens to observe the dynamics of the particle and the other was used to observe and understand the beam profile [7].

Balancing the gradient and scattering forces is an important consideration for optical trapping. To stabilize the trapped nanoparticle further a process called parametric feedback cooling can be employed. Unlike traditional cooling methods that involve atomic or molecular energy levels, parametric feedback cooling dynamically adjusts the forces acting on the particle. This method detects the particle's position in real-time by using an "additional modulation of the sensing laser amplitude".

2.2 Optical Resonators

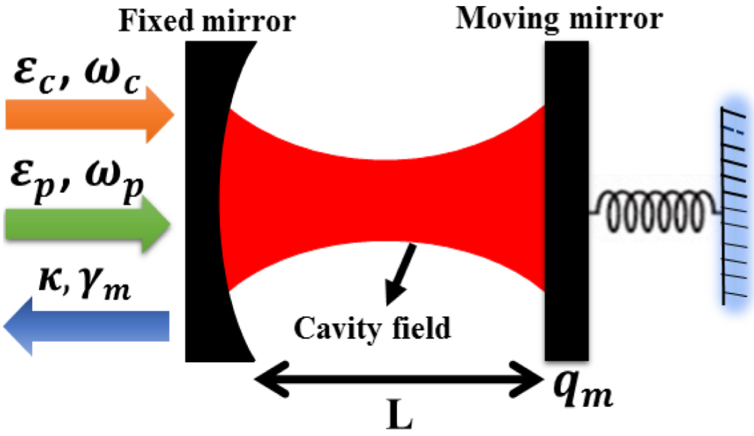

Figure 3: *Schematic diagram of an optical resonator [8].*

An optical resonator, also referred to as an optical cavity, is a common component in several laser optics experiments. The cavity consists of a set of highly reflective mirrors oriented in a way to create a standing wave of light while being confined. This lets the beam to bounce back and forth, increasing the intensity of light inside the cavity.

There are two types of cavities, linear cavities where light bounces back and forth between two highly reflective mirrors and ring cavities where the light can do round trips by going in different directions. This experiment uses a linear optical cavity with two mirrors placed parallel to each other.

Optical cavities are characterized by important parameters such as finesse and free spectral range (FSR). The finesse of a cavity indicates its ability to restrict light based on the reflectivity of its mirrors and the losses within it. The finesse depends entirely on the reflectivity of the mirrors. In contrast, the FSR determines the distance between the cavity's resonant modes, which is critical for frequency tuning in lasers and other optical devices. The FSR can be written as

$$FSR = \frac{c}{2L} \tag{1}$$

where c is the speed of light in vacuum and L is twice the physical length of the resonator. There is no factor 2 for a ring resonator because there is no double pass.

2.2.1 Resonator modes

Optical cavities support specific electromagnetic field configurations called modes. They depend on the cavity's geometry and boundary conditions imposed by the mirrors. These modes can be categorized into longitudinal and transverse modes. Longitudinal modes describe standing waves along the cavity's axis while transverse modes shows the variations in the beam profile perpendicular to the cavity axis and are labeled as TEM_{nm} where n and m represent the number of modes in the horizontal and vertical directions, respectively.

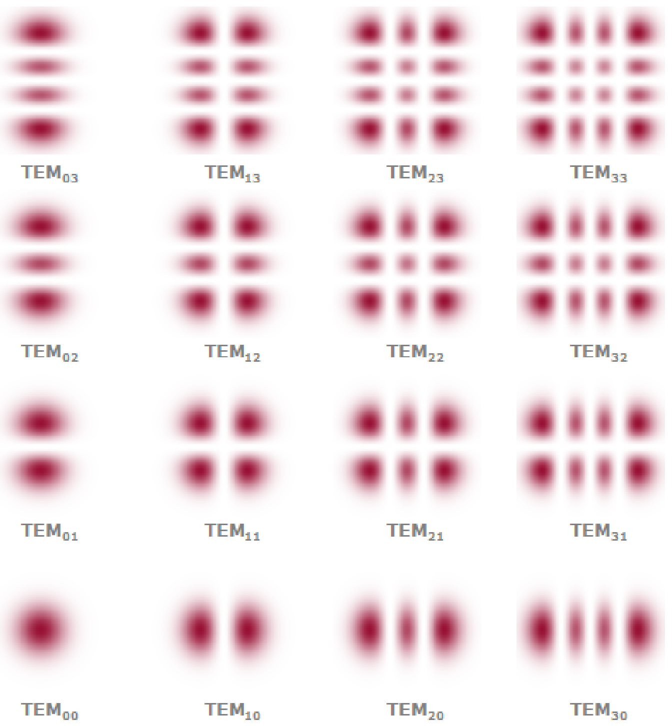

Figure 4: *Different TEM$_{00}$ modes [9].*

Figure 4 depicts the different resonator modes that may arise. The simplest are the fundamental TEM$_{00}$ modes which are known as Gaussian modes. There are also higher order Hermite–Gaussian modes with more complicated distributions. However, this experiment will focus on the fundamental TEM$_{00}$ mode.

2.3 Gaussian Beam Profile

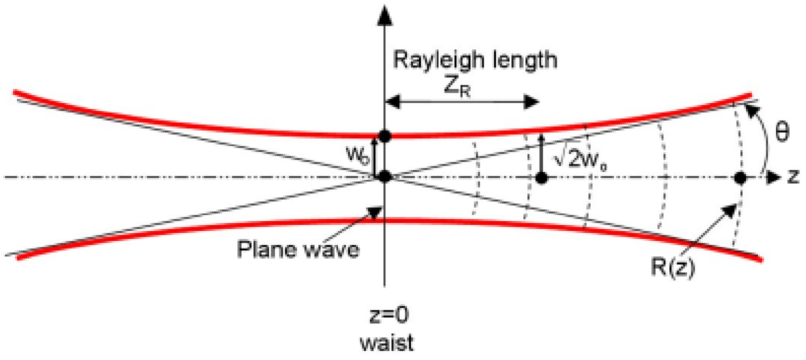

Figure 5: *Properties of Gaussian beam [10].*

A Gaussian beam node assumes that the distance that the rays travel is much larger or much smaller than the Rayleigh range of the beam and that the beam divergence is small.

The electric field amplitude of a Gaussian beam is expressed as

$$\mathbf{E}(\rho, z) = E_0 \frac{\omega_0}{\omega(z)} e^{-\frac{\rho^2}{\omega(z)^2} + \mathbf{i}\phi(\rho, \mathbf{z})} \hat{\mathbf{n}} \tag{2}$$

As mentioned above, this section will focus on situations where the beam divergence is small so that the paraxial approximation can be applied. This approximation allows for omission of the second-order derivative in the propagation equation. The project uses a tightly focused beam which is very similar to a Gaussian beam described by using paraxial approximation [11].

The key parameters defining a Gaussian beam are the beam waist, Rayleigh range, divergence angle, and beam radius. The beam profile is symmetric around the center and decreases as the distance from the center increases. The distribution is defined as:

$$I(r) = I_0 \exp\left(-\frac{2r^2}{w(z)^2}\right) = \frac{2P}{\pi w(z)^2} \exp\left(-\frac{2r^2}{w(z)^2}\right) \tag{3}$$

where I_0 is the peak irradiance at the center of the beam, $\omega(z)$ is the radius of the laser beam and r is the radial distance from the axis.

$$w(z) = w_0 \sqrt{1 + \frac{z^2}{z_0^2}} \tag{4}$$

$$R(z) = z\left(1 + \frac{z_0^2}{z^2}\right) \tag{5}$$

$$\phi(z, r) = k - \eta(z) + \frac{kr^2}{2R(z)} \tag{6}$$

$$\eta(z) = z\left(1 + \frac{z_0^2}{z^2}\right) \tag{7}$$

where $R(z)$ is the radius of curvature of the beam's wavefront at a distance z from the beam waist, $\eta(z)$ is the Gouy phase shift, a phase anomaly that occurs as the beam propagates through the focus and $\phi(z, r)$ is the phase term that accounts for both the propagation and the radial components.

The mathematical description above provides insight into the behavior of Gaussian beams as they propagate through space. To further illustrate these parameters, Figure 6 shows the transverse intensity distribution of the Gaussian beam. The beam exhibits a symmetric intensity profile, with the maximum irradiance I_0 occurring at the center ($r = 0$). As the radial distance increases, the intensity decreases exponentially, as described by Equation 3.

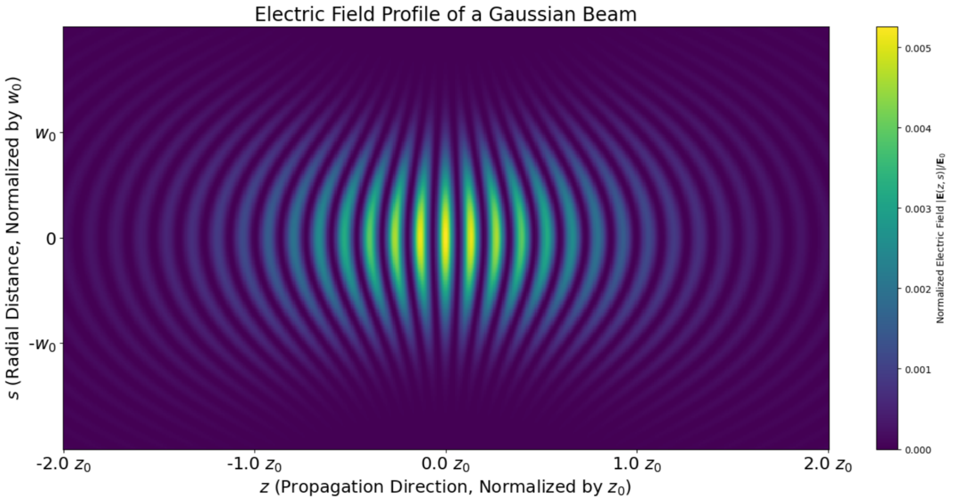

Figure 6: *Gaussian beam profile of an optical tweezer. The maximum intensity is at the center which is where the nanoparticle would be trapped.*

Contrary to the image above, the beam profile in a cavity, in figure 7, has a standing wave structure. This is due to the constructive and destructive interference of the counter-propagating beams inside the resonator. This allows for multiple trapping points since the high intensity antinodes are ideal for trapping nanospheres.

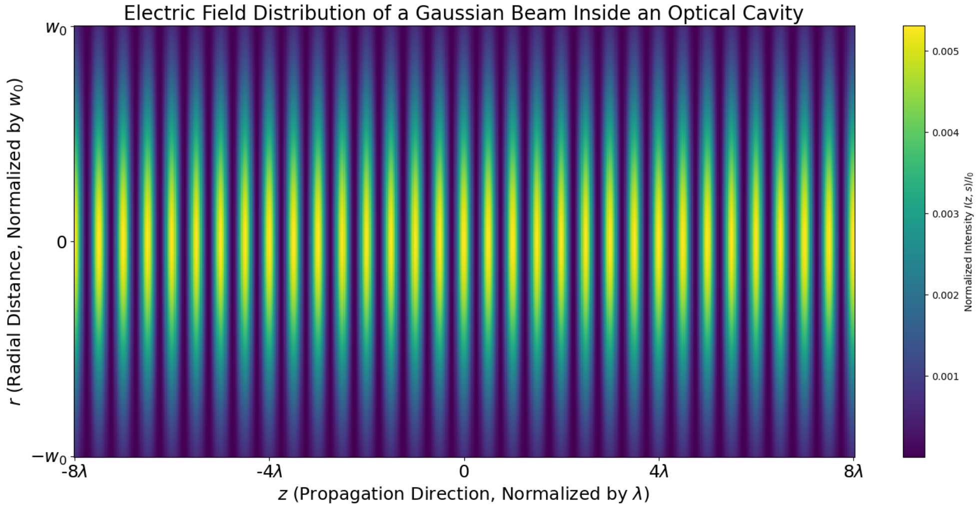

Figure 7: *Gaussian beam profile inside an optical cavity. This images depicts an interference pattern that forms a lattice-like structure where the nanospheres can be trapped at every anti-node due to constructive interference. This supports multiparticle trapping in contrast to the single particle trapping in optical tweezers.*

The amplified intensity inside the cavity increases the depth of these optical potential wells ensuring stable trapping even in the presence of environmental disturbances.

2.4 Optical Forces

Optical forces arise from the interaction of light with matter, driven by the momentum transfer of photons when they interact with dielectric particles. These forces are central to trapping silica nanospheres in an optical cavity and can be categorized into gradient forces and scattering forces, each contributing differently to the stability and dynamics of optical trapping.

$$\mathbf{F}_{\text{optical}} = \mathbf{F}_{\text{gradient}} + \mathbf{F}_{\text{scattering}} \tag{8}$$

2.4.1 Gradient Force

The gradient force which, in contrast to the scattering force, is attractive and arises from the interaction of the induced dipole and the inhomogeneous field

$$\mathbf{F}_{\text{gradient}} = \frac{2\pi\alpha}{cn_m^2}\nabla I_0, \tag{9}$$

where α is the polarizability of the sphere. It can written as

$$\alpha = n_m^2 a^3 \left(\frac{m^2-1}{m^2+2}\right) \tag{10}$$

When the refractive index of the particle is higher than that of the surrounding medium ($m > 1$) the gradient force pulls the particle toward regions of higher light intensity, such as the center of a focused beam. This ensures that the particle is confined within the optical trap, as the force naturally directs it up the intensity gradient.

2.4.2 Scattering force

The scattering force arises due to the radiation pressure on the particle which can be absorbed or re-emitted by atoms and molecules. This force is in the direction of propagation of the incident light and is generally repulsive [12]. For a sphere with radius a

$$\mathbf{F}_{\text{scattering}} = \frac{I_0 \sigma n_m}{c} \tag{11}$$

where I_0 is the intensity of incident light, n_m is the index of refraction with σ being the scattering cross section

$$\sigma = \frac{128\pi^5 a^6}{3\lambda^4}\left[\frac{m^2-1}{m^2+2}\right]^2 \tag{12}$$

where m is the ratio of the index of refraction of the particle to the index of the medium and λ is the wavelength of the trapping laser [13].

2.4.3 Balancing Gradient and Scattering Forces

Optical trapping requires the gradient force $\mathbf{F}_{\text{gradient}}$ to dominate over $\mathbf{F}_{\text{scattering}}$ as the gradient force pulls the particle towards regions of higher light intensity such as focal points, whereas the scattering force pushes the particle along the direction of light propagation, potentially destabilizing the trap.

Techniques like using a tightly focused beam and choosing a wavelength to maximize polarizability while minimizing scattering enhances the gradient force. Reducing particle size and using linearly polarized light can help minimize the scattering force as smaller particles reduce the scattering cross section σ according to the Rayleigh scattering approximation [14].

2.5 Side-of-Fringe Locking

Side-of-Fringe locking is a straightforward and simple way to lock a cavity. It involves maintaining the laser frequency on the slope of a cavity's transmission fringe. Small changes in laser frequency leads to large changes in transmitted light intensity. An automated locking system is used to have a setpoint on one side of the fringe so that the intensity at that point is about half of the resonance peak. The setpoint is given by a reference voltage V_{set} that has a certain frequency which can be used to alter voltage that is obtained from the transmission signal V_T. A piezoelectric actuator, explained in section 3.1.1, is used to account for the laser frequency drifts to maintain long-term locking.

This setup provides the easiest way to obtain an error signal. Like any other locking method this has its advantages and disadvantages. There is no modulation required to stabilize the laser to the side of the peak [15]. However, this could lead to significant unwanted noise in the error signal. It could also be time consuming to implement the locking process itself since this method uses a small acquisition range which means that laser frequency already needs to be near resonance for it to lock. This system is also prone to environmental disturbances such as sound and other mechanical vibrations that might cause the laser frequency to unlock.

Some of these issues can be mitigated slightly by using a high finesse cavity and a low pass filter to filter out high frequency noise. However PDH locking, explained in the next section, fixes the drawbacks mentioned by modulating the laser.

2.6 Pound-Drever-Hall (PDH) Locking

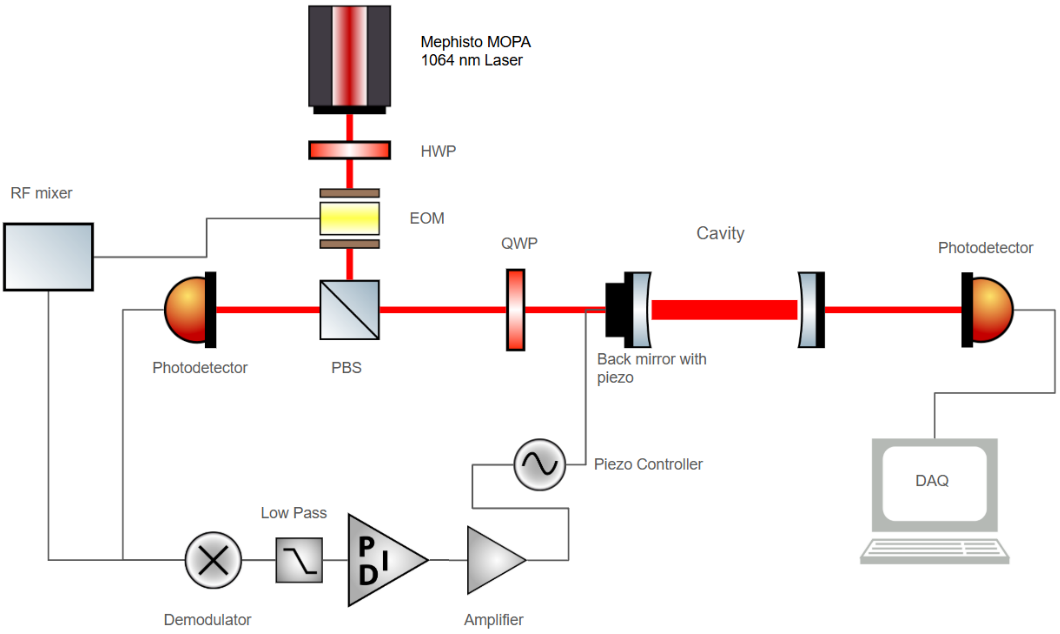

Figure 8: *Experimental setup of PDH locking.*

Pound-Drever-Hall (PDH) Locking is a technique that is used for stabilizing the cavity. A crucial component of the PDH locking technique is the Electro-Optic-Modulator (EOM) which modulates the phase of the laser at a fixed frequency ω_m which in turn creates sidebands around the carrier, given by $\omega_0 \pm \omega_m$ with ω_0 being the carrier frequency, that do not resonate with the cavity so that the light almost entirely reflects back. The light from the laser with frequency that matches the cavity resonance enters the cavity while the light that is off-resonance is reflected and contains interference patterns between the carrier and the sidebands.

The reflected light from the cavity contains information about the phase which shows the mismatch between the laser and the cavity. However just looking at the intensity of the light would not be enough to figure out if the frequency is lower or higher than the cavity resonance frequency since the intensity is symmetric about resonance. This light is passed onto a photodetector and the resulting signal is multiplied with a reference signal at the same modulation frequency and phase as the EOM. The process of modulating and demodulating the signal allows for measurement of the slope of the derivative of the resonance curve, as seen in figure 9, to determine if the laser's frequency is higher or lower than the resonance and how far it is off by. This goes into a low-pass filter to obtain a DC component which is the error signal. This error signal is sent to a PID (Proportional–Integral–Derivative) controller which uses a Piezoelectric actuator that controls the cavity length by fine-tuning the distance between the mirrors or a current modulator which adjusts the laser frequency via injection currents.

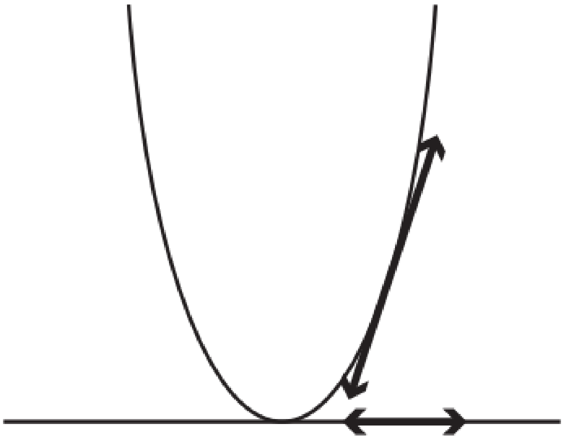

Figure 9: *Intensity of reflected light. The offset of frequency can be determined by looking at which side of resonance it is on [16].*

2.6.1 Sidebands

The PDH locking technique employs phase modulation to create sidebands around the laser's carrier frequency which is crucial for error signal generation. Applying modulation to the laser generates sidebands. This can be achieved by using an AOM or EOM. The phase modulated electric field can be written as

$$E_{\text{inc}} = E_0 e^{i(\omega t + \beta \sin \Omega t)} \tag{13}$$

Expanding this using Bessel functions

$$E_{\text{inc}} \approx \left[J_0(\beta) + 2iJ_1(\beta)\sin\Omega t\right] e^{i\omega t} = E_0 \left[J_0(\beta)e^{i\omega t} + J_1(\beta)e^{i(\omega+\Omega)t} - J_1(\beta)e^{i(\omega-\Omega)t}\right] \tag{14}$$

where Ω is the phase modulation frequency and β is the modulation depth [17]. The power in the carrier is

$$P_c = J_0^2(\beta)P_0 \tag{15}$$

when the power of the incident beam is given by $P_0 \equiv |E_0|^2$, where E_0 is the electric field amplitude. The power in the first-order sideband would be

$$P_s = J_1^2(\beta)P_0 \tag{16}$$

For large modulation depths ($\beta \geq 1$) power is distributed across higher-order sidebands which may reduce the efficiency of the locking. For small modulation depths ($\beta < 1$) most of the power remains in the carrier and first-order sidebands [17],

$$P_c + 2P_s \approx P_0. \tag{17}$$

2.6.2 Demodulation and Error Signal Extraction

After the generation of sidebands, the phase mismatch information in the interference is isolated between the carrier and sidebands. This process is known as demodulation. This error signal provides real-time feedback about whether the laser frequency is above or below the cavity resonance. When a phase-modulated beam is reflected from the optical cavity, it contains three distinct frequency components: the carrier frequency ω and the sidebands at $\omega \pm \Omega$, where Ω is the modulation frequency applied by the EOM. The reflected electric field can be written as:

$$E_r = R_c E_0 e^{i\omega t} + R_+ E_0 e^{i(\omega+\Omega)t} + R_- E_0 e^{i(\omega-\Omega)t} \tag{18}$$

where R_c, R_+, and R_- are the reflection coefficients for the carrier and sidebands, respectively. The intensity of the reflected field, which is proportional to the square of the electric field magnitude, is given by:

$$I_r \propto |E_r|^2 = |R_c|^2 + |R_+|^2 + |R_-|^2 + 2\mathrm{Re}[R_c R_+^* e^{i\Omega t}] + 2\mathrm{Re}[R_c R_-^* e^{-i\Omega t}]. \tag{19}$$

2.7 Other locking methods

This experiment employs the Pound-Drever-Hall (PDH) Locking method, however there are other locking techniques worth exploring that may help with the limitations that PDH locking faces.

2.7.1 Hänsch–Couillaud

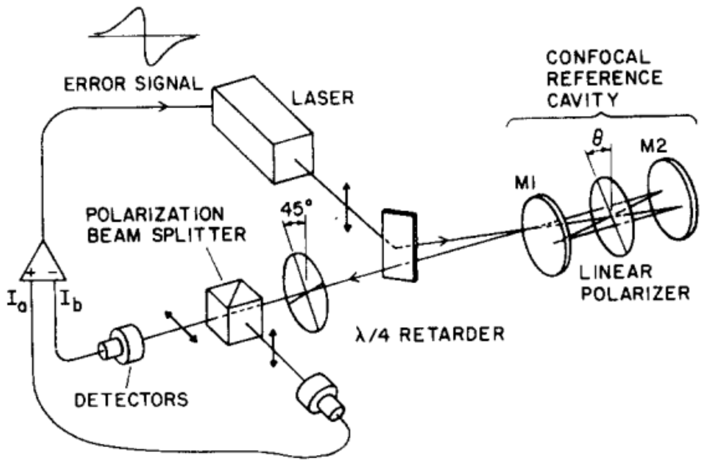

Figure 10: *Laser frequency stabilization in Hänsch–Couillaud locking technique [18].*

The Hänsch–Couillaud locking method was first introduced in 1980 by T.W. Hänsch and B. Couillaud. This technique involves a linear polarizer placed inside a cavity so that the reflected light is elliptically polarized [18]. Unlike PDH locking which relies on phase modulation Hänsch–Couillaud locking modulates the polarization state of the laser. If the laser frequency is off resonance with the cavity then the reflected light will contain two orthogonal polarization components with a phase difference. The field amplitudes of these two components are expressed as

$$E_{\parallel}^{(i)} = E^{(i)} \cos\theta, \quad E_{\perp}^{(i)} = E^{(i)} \sin\theta \tag{20}$$

They are separated by a polarizing beam splitter and the relative intensities are detected using a differential photodetector. The perpendicular component is reflected back while the parallel component undergoes a phase shift, thus acquiring an elliptical polarization. The two outputs are measured by photodetectors which is connected to a differential amplifier. At resonance, the intensity difference would be 0 and the polarization is linear. The error signal is proportional to the intensity difference which can be written as

$$I_a - I_b = I^{(i)} 2\cos\theta \sin\theta \frac{T_1 R \sin\delta}{(1-R)^2 4R \sin^2\frac{\delta}{2}}. \tag{21}$$

While this method proposes a somewhat straightforward and simple approach to laser frequency stabilization, it has its pros and cons. One advantage of this technique is its simplicity as it does not require the use of an AOM or EOM. However, this is only beneficial for low finesse cavities since the polarization effects are more pronounced there. This method is sensitive to polarization drifts that can be caused by various environmental factors such as mechanical vibrations or thermal fluctuations.

2.7.2 Frequency Modulation (FM) Spectroscopy

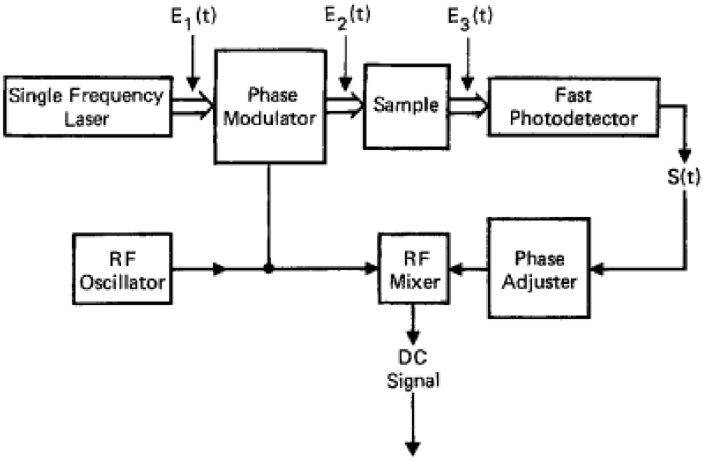

Figure 11: *Frequency Modulation (FM) Spectroscopy [19].*

In contrast to the phase modulation techniques explained in previous sections, this setup changes the instantaneous frequency of the wave. Frequency modulation has various applications, such as telecommunications and signal processing. The laser frequency is sinusoidally modulated at a frequency Ω which creates sidebands around the carrier frequency at $\omega \pm \Omega$, similar to the sideband generation in PDH locking. A single-mode dye laser is used in order to have less noise [19]. The transmitted and reflected signals contain information about the resonance. The system's response to the modulated frequency is then detected using a phase-sensitive detection (PSD) method.

FM spectroscopy does not require a cavity, making it easier to implement the method for atomic and molecular spectroscopy. This method is also very sensitive to resonance features and provides excellent signal-to-noise ratios.

3 Experimental Methods

Trapping of nanoparticles relies on the interaction of light and dielectric particles. The methods involve scanning and locking the cavity to investigate the resonance characteristics and assess the quality of the cavity for future trapping experiments.

3.1 Cavity Scanning

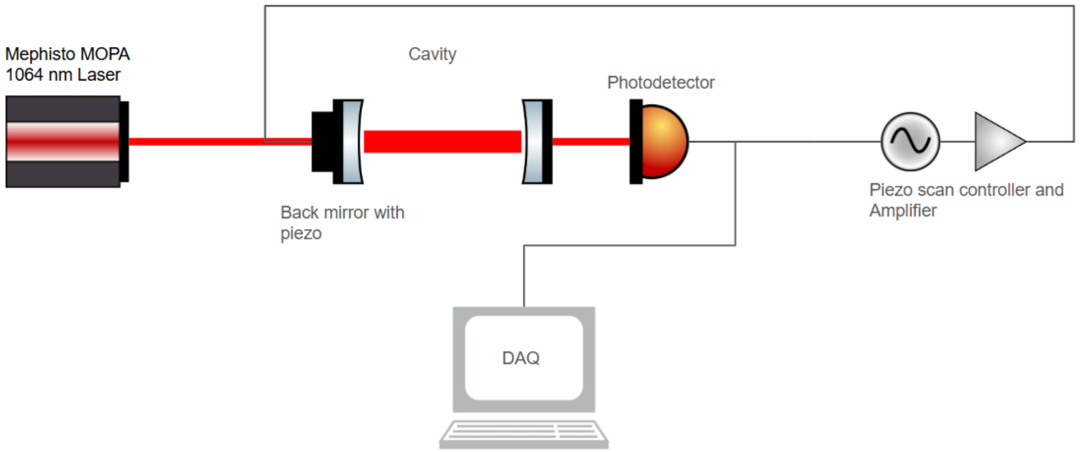

Figure 12: *Experimental setup for scanning the cavity.*

Cavity scanning is a technique used to probe the optical resonance characteristics of a cavity by varying its effective length. By varying the cavity length, it alternates between resonance and off-resonance conditions. A Toptica SC110 scan control module was used to scan the cavity. A Thorcam was placed above the cavity to observe the reflection on the back mirror for alignment of the cavity to obtain resonance. A 1064 nm TEM_{00} laser on full power was used to deliver a clean Gaussian beam profile. The front mirror was attached to a piezoelectric actuator which will be discussed in the later sections. The setup also included half-waveplates and quarter-waveplates which rotate the polarization and they are adjusted depending on the requirement. A polarizing beam splitter is placed after the half-waveplate to split the beam into 2 parts.

The cavity is placed inside a vacuum chamber to allow for future trapping experiments. The cavity consists of two high reflectivity mirrors placed parallel to each other reflecting about 99.44% of the light. The light goes through an EOM into a half-wave plate to polarize it before it goes into a polarizing beam splitter (PBS). This light then sent into the cavity through a quarter-wave plate to convert the linearly polarized beam into circularly polarized light to improve coupling into the cavity. The light reflected from the cavity can be collected by using the same PBS to send the beam into a photodiode to obtain valuable information about the laser beam to create sidebands and eventually lock the cavity. However, in this experiment only scanning was performed.

The laser that was used was a Mephisto MOPA Nd:YAG 42 Watt infrared laser which emits light at 1064 nm. The Gaussian beam profile that was obtained with the laser on full power allowed for efficient coupling into the cavity, maximizing the transmitted light signal and resonance stability. At 1064 nm, the beam is invisible to the naked eye, which was why additional safety precautions such as protective eyewear were taken to prevent accidental exposure.

3.1.1 Piezoelectric Actuator

A piezoelectric actuator is a transducer which converts electric signals into controlled displacements. These devices are used for applications that require ultra-precision and high force handling. Piezo actuators have a few important specifications that need to be considered which are force, displacement and operating voltage. Additional factors that can affect the performance are capacitance, stiffness and resonant frequency.

Stiffness governs how much energy is required for a certain deformation. The capacitance is related to the excited voltage frequency while the resonance is the frequency where the Piezo actuator reacts with the highest amplitude.

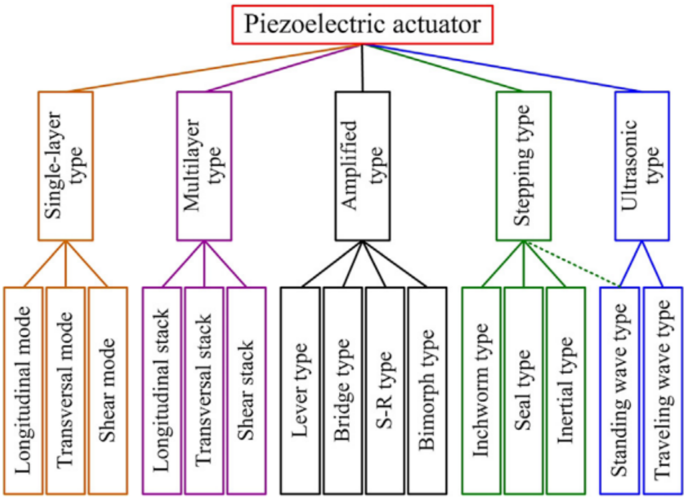

Figure 13: *Different types of piezoelectric actuators [20].*

Figure 13 shows the classifications of piezo actuators. In some cases of single-layer piezoelectric actuators, the deformation is too small to be applied in most experiments [21]. Stacking up multiple single-layer piezo actuators with all the deformation orientations being in the same direction solves this issue. Piezo-stack actuators, with the electrodes connected in parallel, stack up all the small deformations to have a large displacement.

However, even the piezo-stack actuators cannot deliver the required displacement in some cases. Using too many single-layer actuators to fix this problem leads to new ones such as size and dimensional issues. Amplified actuators use a mechanism called flexure hinge, also called flexural pivot, that is widely used in applications that involve ultra-precision.

Flexure hinges work on the same principle, their elastic structure deforms when forces are applied. They have several advantages such as the fact that they are virtually frictionless and have very low inertial mass.

In experiments that require that require displacements of a few millimeters need a new mechanism that provides larger deformation. Stepping actuators are a type of piezoelectric actuator designed to achieve long travel ranges while maintaining the high precision characteristic. These actuators use a stepwise motion mechanism to achieve extended travel. One part of the actuator clamps to the moving element while the other remains stationary. Then the clamp releases whereas the other stabilizes the motion. The peizo actuator then contracts to pull the back end further. This sequence is repeated to achieve cumulative motion.

The last type of actuator is the Ultrasonic actuator which, in contrast to previous working principles, utilizes high-frequency oscillations in the ultrasonic range (20kHz-200kHz) to generate motion. The piezoelectric material in the actuator vibrates at its resonance frequency when subjected to electric signals. These high-frequency vibrations are transformed into motion using frictional coupling between the vibrating actuator and a movable element. This actuator can be classified into standing wave actuators, where vibrations create nodes and antinodes which drive the movement, and travelling wave actuators which uses a continuous travelling wave that propagates through the piezo material and carries the movable part that presses against the actuator. This information was obtained from "A survey of piezoelectric actuators....." by Shupeng Wang et al [20] which is a comprehensive guide to the different types of piezoelectric actuators.

3.1.2 Waveplates

The two waveplates that were used in the setup were half-waveplate and quarter-waveplate. Their goal is to control the polarization to optimize interaction with other components such as the PBS and optical cavities. Waveplates are made from birefringent materials which have different indices of refraction in different orientations. They have a fast axis and a slow axis to control the speed of light traveling through them depending on which axis it goes through.

Half-waveplates rotate the polarization of linearly polarized light. The rotation angle is determined by the orientation of the waveplate's fast axis relative to the incoming polarization. In this experiment, the HWP was used to align the polarization of the laser beam with the PBS's splitting axis. It was placed after the EOM, before the PBS.

Quarter-waveplates, on the other hand, turn linearly polarized light into circularly polarized light and vice versa. Circular polarization can improve the interaction of light with certain optical elements, such as the cavity mirrors. The QWP in this setup was used to improve the coupling of the laser beam into the cavity. It is typically placed before the cavity.

3.2 Fringe Locking

Side-of-Fringe locking, as explained in section 2.5, was fairly and simple to implement. The setup included a PID (Proportional-Integral-Derivative) controller connected to DigiLock to produce an error signal.

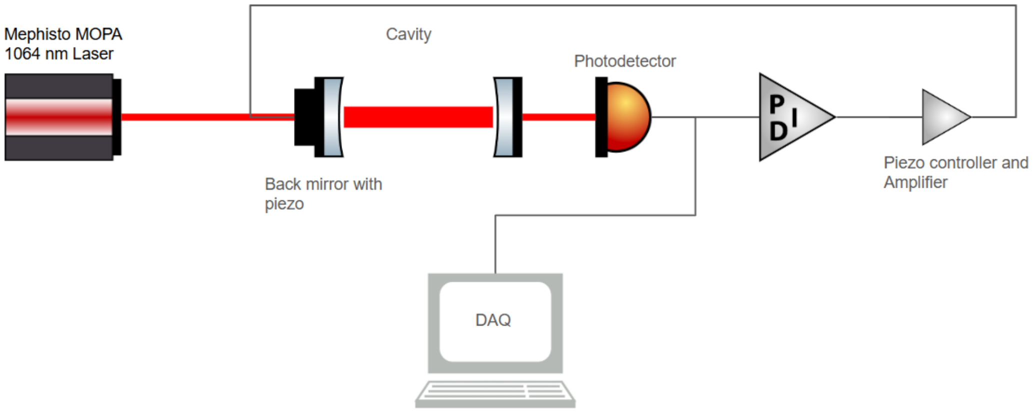

Figure 14: *Experimental setup of side-of-fringe locking.*

Figure 14 shows the setup of the side-of-fringe locking mechanism. The transmitted signal is picked up by a photodetector and sent to the PID which is connected to a DigiLock that has an autolock system. The signal is observed on a Picoscope. Scanning is performed by the piezo actuator to observe the resonance of the cavity. Once the TEM_{00} peak is obtained a setpoint of some voltage is selected to center it. The feedback signal from the PID controller is sent to an amplifier which outputs up to 150 V. This high voltage signal is then sent back to the piezo actuator which expands and contracts to stabilize the laser to lock on to the resonance of the cavity.

A low pass filter can be used to filter out the high frequency noise although that was not required in this setup as the signal-to-noise ratio was sufficient already.

3.3 Data Acquisition

In this experiment, the system was designed to record transmitted light to extract meaningful information about resonance peaks, signal-to-noise ratio and other key metrics. This section explains the major tools and components involved used for data collection and signal processing.

The transmitted light was collected by a photodiode which converts the light from the cavity into electrical signals. Another photodiode is also used to monitor the backreflected light to generate an error signal for PDH locking. Althought this experiment focused on scanning, the backreflected light could be used to lock the cavity for future experiments. The electrical signals from the first photodiode were fed into a high-resolution Picoscope for recording in the time domain. This oscilloscope (Picoscope) worked as the central data acquisition tool with a sampling rate of 20 MS, enough to capture fast oscillations in the cavity signal. This setup enabled simultaneous recording of transmitted light and the synchronization trigger (Channel A). The trigger acted as a clock signal to synchronize the data with the piezoelectric actuator's voltage ramp. Channel D captured the intensity of transmitted light, where periodic peaks corresponded to cavity resonance conditions.

4 Results and Discussion

The results presented in this section focus on the characterization of the optical cavity, a critical step toward achieving stable trapping of silica nanospheres. The cavity was scanned using a piezoelectric actuator (PZT) to identify resonant modes and assess its performance. Data were collected using a Picoscope and analyzed to determine the cavity's transmission profile and stability. These results provide insights into the cavity's suitability for trapping and potential areas for optimization.

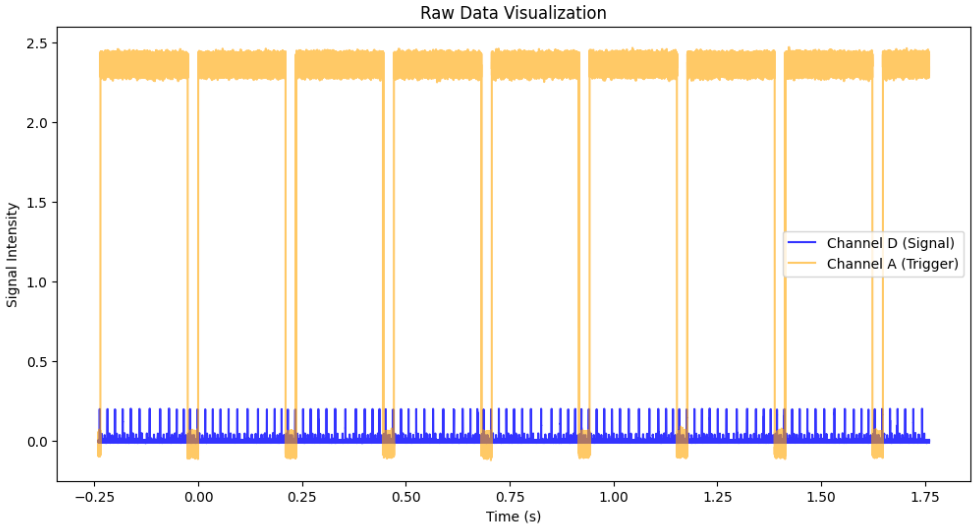

Figure 15: *Raw data that was obtained using a picoscope.*

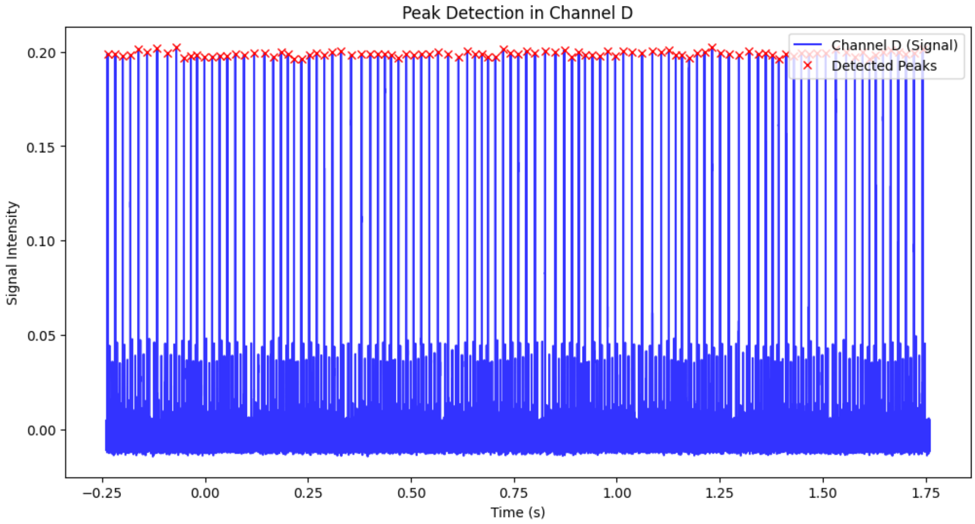

Figure 16: *Data of scanning a cavity with peaks detected.*

Figures 15 and 16 show the raw data that was obtained from scanning the cavity. Channel A represents the trigger signal acting as a trigger while Channel D is the signal from the cavity. The periodic peaks in Channel D correspond to resonance conditions where the cavity length $L = \frac{m\lambda}{2}$ where m is the mode number.

This section focuses on peak detection, signal-to-noise ratio, FSR calculations for characterizing and inferring the properties of the cavity.

4.1 Resonance Peak Detection

The periodicity of resonance peaks in the cavity arising from constructive interference is characterized by the free spectral range (FSR). This is a critical parameter for understanding cavity's performance. It was found that in a time span of 2 seconds there were 102 detected peaks. The average time spacing between consecutive peaks was calculated to be 0.0196 seconds.

Resonance peaks were identified in the cavity signal using the `find_peaks` algorithm. Peaks were defined as points with amplitudes above a threshold of 0.1 separated by atleast 500 points to avoid spurious detections. The average spacing between points in the time domain was calculated to be 58 Hz.

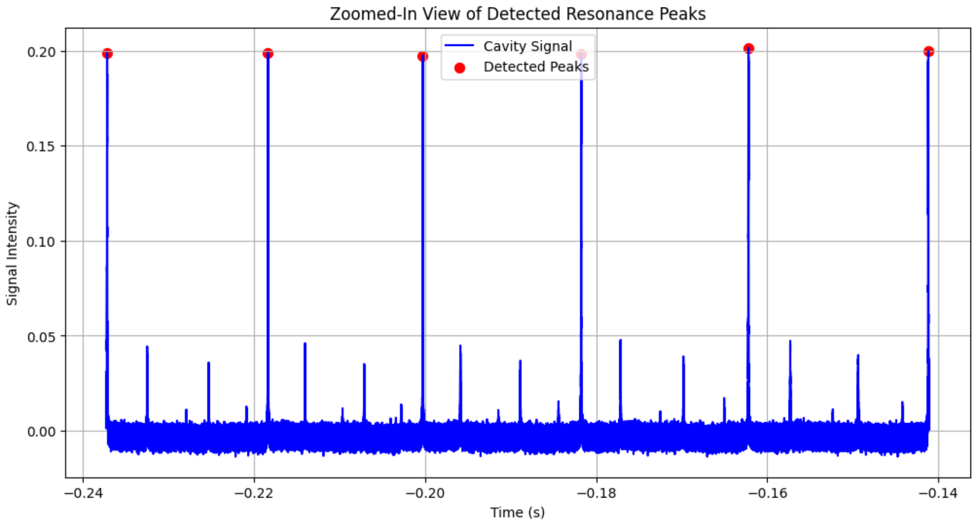

Figure 17: *Zoomed-in view of the first 6 peaks detected.*

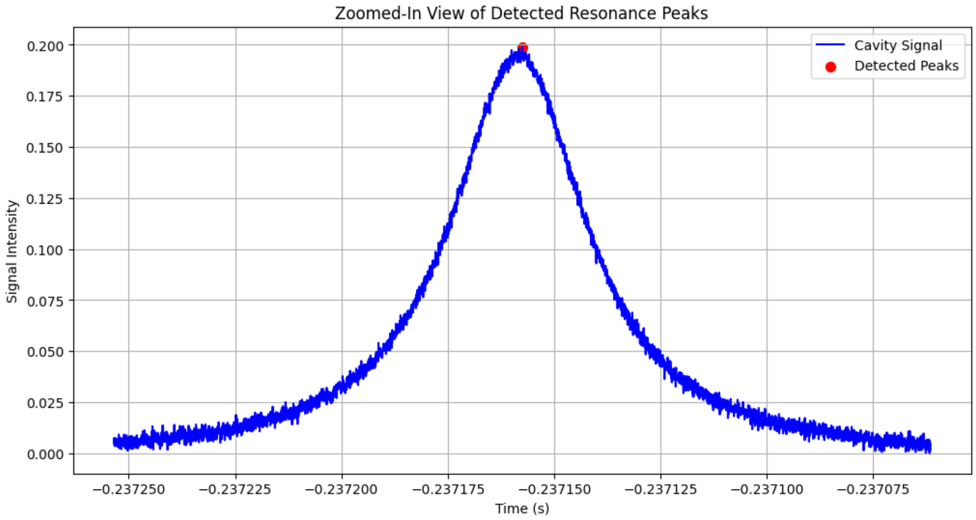

Figure 18: *Zoomed-in view of a single detected peak.*

Figures 17 and 18 provide the zoomed-in view of the resonance peaks, showing the sharpness and regularity. These observations demonstrate that the measurements accurately reflects the cavity's resonance behavior. However it can be noticed in Figures 16 and 17 that the peaks are not evenly spaced apart. Using a Python script it was found while the peaks had a standard deviation of 0.002789 s from the mean of 0.0196 s.

4.2 Signal-to-Noise Ratio Analysis

This section evaluates the stability of the cavity signal. The signal-to-noise ratio (SNR) is a measure of resonance signal to the baseline noise. A high SNR indicates a clear and stable signal. The ratio can be expressed as

$$SNR = \frac{A_{peak}}{\sigma_{noise}} \tag{22}$$

Here A_{peak} is average resonance peak height and σ_{noise} is the standard deviation of the baseline noise. Using a Python script, A_{peak} was found to be 0.187 and σ_{noise} was 0.0057. Thus, the SNR was found to be 32.3 which shows that the resonance peaks are clearly distinguishable from the baseline noise. A high SNR is critical for future experiments involving trapping since precise detection is required.

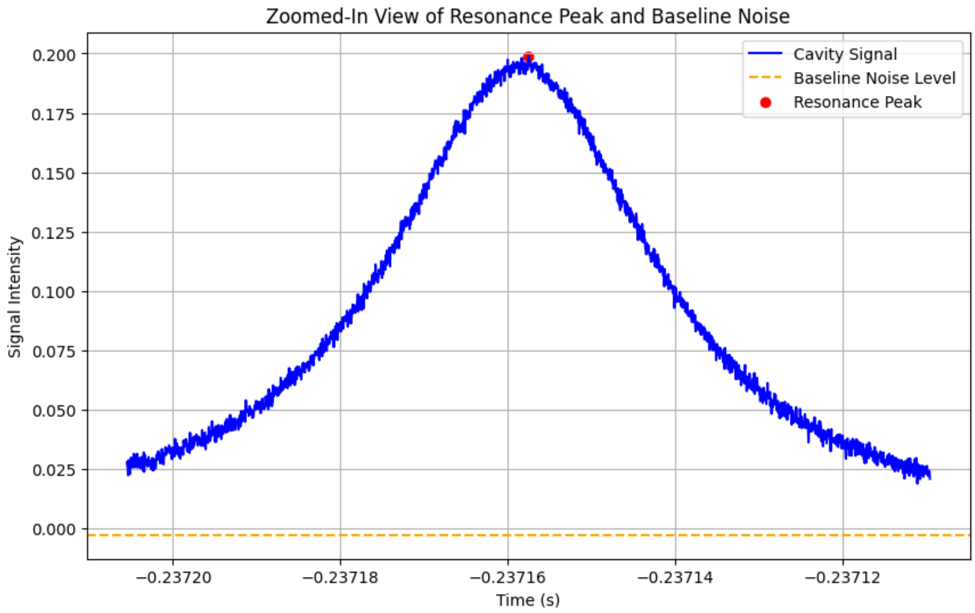

Figure 19: *Signal-to-Noise Ratio.*

As seen in figure 19, the baseline noise is relatively stable compared to the cavity signal which indicates a strong SNR.

4.3 Resonance Linewidth

The linewidth can be defined as the full-width at half-maximum (FWHM) of the resonance curve and has implications for resolution and signal-to-noise ratio. The FWHM is an important parameter that can be used to characterize the quality of an optical cavity. Narrow resonance linewidths indicate high-quality cavities with minimal energy dissipation and high reflectivity of the mirrors. The FWHM is also used to calculate the cavity's quality factor Q which is defined as:

$$Q = \frac{v}{\Delta v} \tag{23}$$

where v is the resonance frequency and Δv is the FWHM in terms of frequency. A higher Q factor indicates that the cavity is well-constructed and aligned and is suitable for advanced applications such as nanoparticle trapping and quantum optics experiments.

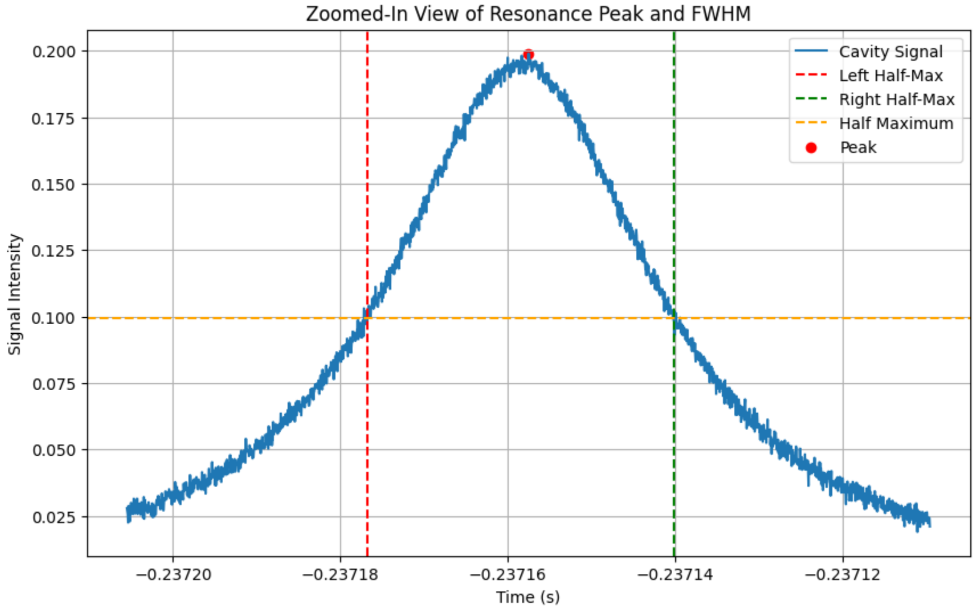

Figure 20: *Zoomed-in view of a single peak depicting the FWHM.*

The FWHM was calculated by identifying resonance peaks using the `find_peaks` as mentioned before. Figure 20 shows a specific peak selected for analysis. The time difference between the right and left points on the signal corresponding to half of the maximum peak intensity is the FWHM. The resulting FWHM, expressed in seconds provides a measure of the resonance linewidth in the time domain. The value was found to be 3.52×10^{-5} seconds. Similar to the peak spacing, the linewidth had an error. This was found to be 5.71×10^{-6} s which is a relative error of 16.24 %.

4.3.1 Finesse

The finesse is a dimensionless indicator of the sharpness of a cavity. It measures how narrow the resonances are compared to their frequency distance. It can be defined as the ratio of the Free Spectral Range (FSR) to the Full Width at Half Maximum (FWHM) of the resonance peaks:

$$\mathcal{F} = \frac{\text{FSR}}{\text{FWHM}} \tag{24}$$

The theoretical value of the FSR for a 19cm cavity would be ≈ 800 MHz using equation 1. However the data was taken recorded in a time domain. Instead of measuring the FSR and FWHM in terms of frequency, the finesse can also be calculated using the time spacing:

$$\mathcal{F} = \frac{\text{Peak Spacing (Time Domain)}}{\text{FWHM (Time Domain)}} \tag{25}$$

The time spacing between peaks was found to be 0.0196 s and the FWHM was 3.52×10^{-5}. This gives a finesse of approximately 557. The peak spacing and the FWHM both have errors, however. The total relative error is calculated to be 21.34 %. This gives a finesse of 557 ± 119. Energy is lost after each round trip inside the cavity. This can be calculated using

$$\mathcal{F} = \frac{\pi\sqrt{r}}{1-r} \tag{26}$$

where r is the reflection coefficient of the mirrors. For a cavity with a finesse of 557 it can be found that 0.56% of light is lost each round trip. The error propagation can be written as

$$\Delta(\text{Loss}) = \left|\frac{d(\text{Loss})}{d\mathcal{F}}\right| \Delta\mathcal{F} \tag{27}$$

which gives us

$$\Delta(\text{Loss}) = \frac{\pi}{\mathcal{F}^2} \cdot \Delta\mathcal{F} \tag{28}$$

Using formula 28 it can be seen that the error in the loss of energy is 0.118%. Therefore, the cavity loses $(0.56 \pm 0.12)\%$ of light each round trip.

4.3.2 Power Buildup

Intensity inside the cavity is built up as light bounces back and forth, losing only a very tiny fraction of light each round trip. If the incident power of the laser is P_0 then the power inside the cavity can be written as

$$P_c = \frac{P_0\mathcal{F}}{\pi} \tag{29}$$

where $\mathcal{F}$ is the finesse of the cavity. The intracavity power build up is defined as the ratio of the power inside to the incident power:

$$\kappa = \frac{P_c}{P_0} = \frac{\mathcal{F}}{\pi} \tag{30}$$

The cavity that was used in this experiment has a finesse of 557 ± 119. Therefore, using equation 29 the power build up factor would be 177.3 ± 37.

4.4 Fringe Locking

This section focuses on the error signal once the cavity is locked in resonance using the side of a fringe. Figure 21 shows a picture of the cavity from bird's-eye view. This picture was taken with a thorcam, zoomed in and adjusted for infrared light.

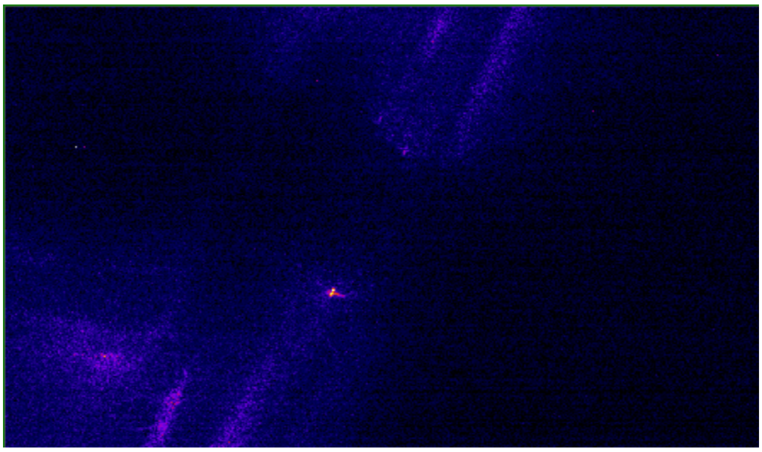

Figure 21: *Image of the cavity while locked on to resonance. The bright spot in the middle depicts the amplification of light inside which bounces off other components in the experimental setup.*

Figure 22 depicts the transmitted light that was generated from locking the cavity. The lock was relatively stable with slight environmental disturbances. The PID controller was used to refine the noisy signal to something that can be used to lock the cavity and provide a reliable feedback system. The DigiLock included the Gain, Proportional, Integral and Derivative terms which can be tweaked to adjust the stability of the lock.

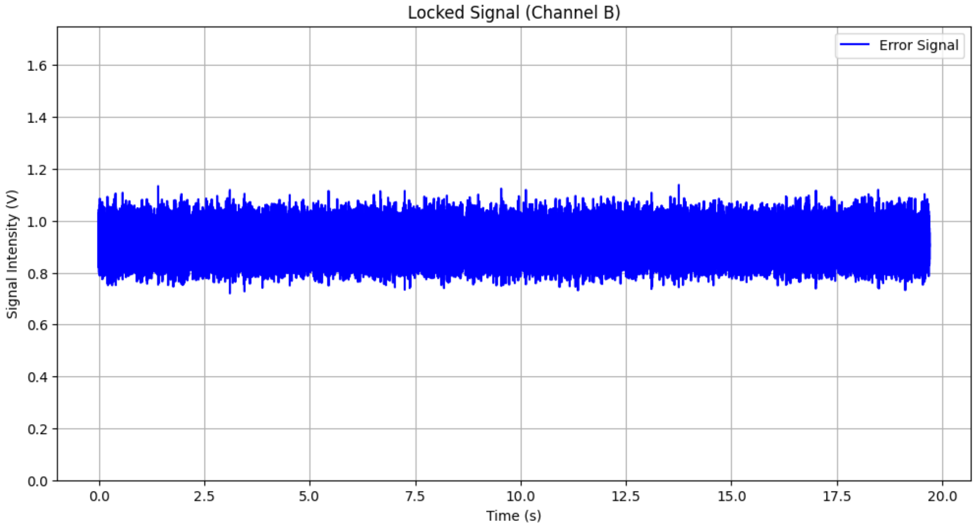

Figure 22: *Feedback signal generated from DigiLock. Deviations in this signal represent how well the PID controller is compensating for external disturbances to maintain resonance.*

It was found that the proportional and derivative terms had no effect on the error signal whatsoever. The optimal ranges for the Gain and Intergal terms were 5-15 and 25-35 respectively. Going outside this range led to failed locking and overcompensating.

4.4.1 Error Analysis

To analyze the stability of the locked signal the mean value and the root mean square (RMS) error were calculated. This was done using a Python script. These metrics can provide some insight into the accuracy and fluctuations of the setup. The mean value represents the average signal intensity over the entire duration of the dataset which can be written as

$$\mu = \frac{1}{N} \sum_{i=1}^{N} x_i \tag{31}$$

where N is the total number of data points and x_i represents the i^{th} signal intensity value. From the data it was calculated to be $\mu = 0.9139V$. The root mean square error σ_{RMS} is defined as the deviation of the signal from its mean value. It can be written as

$$\sigma_{\text{RMS}} = \sqrt{\frac{1}{N} \sum_{i=1}^{N} (x_i - \mu)^2} \tag{32}$$

σ_{RMS} was found to be 0.0462 V. This is approximately an error of 4.6%, demonstrating good stability in the locking process.

5 Conclusion

The first part for the experiment was analyzing the characteristics of an optical cavity as a preparatory step for trapping silica nanospheres inside a vacuum chamber. The cavity was first aligned using two highly reflective mirrors and observing resonance through a camera lens and was later scanned using a Toptica piezo controller.

A total of 102 peaks were detected over a 2-second interval and the peaks had a linewidth of $3.52 \times 10^{-5} \pm 5.71 \times 10^{-6}$ seconds. These experimental results were used to calculate the finesse of the cavity, by working out the ratio of the distance between the peaks and the width of a peak itself. The finesse was found to be 557 ± 119 which subsequently means the reflectivity of the mirrors is $(99.32 - 99.56)\%$. $(0.56 \pm 0.12)\%$ of light is lost each round trip indicating the high reflectivity of the mirrors and stability of the cavity. The large errors could have been caused by mode mismatches, cavity misalignment or residual air or dust in the cavity.

The second part of the experiment was locking the cavity using Side-of-Fringe locking where one can autolock the cavity to the side of the selected fringe. It was found that this method was prone to environmental disturbances such as mechanical vibrations and sound. It was found that this locking method generated an error signal with a standard deviation of 4.6% from the mean of the signal. This number may be reduced by conducting the experiment in a quieter environment and more efficient tools.

The stable and well-characterized cavity demonstrated here can be used in future experiments to explore critical aspects of trapped particles, such as their thermal motion, interaction with cavity modes, and response to external forces. The standing wave structure of the cavity allows for the potential of trapping multiple particles simultaneously compared to the single trap in the case of optical tweezers. The next steps would be to implement PDH locking and then finally replacing optical tweezers with optical resonators for trapping.

6 Acknowledgments

I would like to sincerely thank Steven Hoekstra for welcoming me into his research group, especially at an unusual stage. I loved our weekly meetings where I had the chance to listen to PHD students in the group talk about their interesting work and other scientific advancements across the world.

Secondly, I want to thank Bart Schellenberg for answering my countless questions and for going out of his way to help me with my project. It has also been a pleasure working with Pablo, the other BSc student in the group. This project has honestly been a breath of fresh air after a lot of theoretical work throughout the physics programme.

7 References

[1] P. N. Lebedev, "Experimental examination of light pressure," Tech. Rep., p. 433.

[2] E. F. Nichols and G. F. Hull, "A Preliminary Communication on the Pressure of Heat and Light Radiation," *Physical Review (Series I)*, vol. 13, no. 5, pp. 307–320, Nov. 1901, ISSN: 1536-6065. DOI: 10.1103/PhysRevSeriesI.13.307.

[3] D. S. Bradshaw and D. L. Andrews, "Manipulating particles with light: radiation and gradient forces," *European Journal of Physics*, vol. 38, no. 3, p. 034 008, May 2017, ISSN: 0143-0807. DOI: 10.1088/1361-6404/aa6050.

[4] A. Ashkin, "Acceleration and Trapping of Particles by Radiation Pressure," *Physical Review Letters*, vol. 24, no. 4, pp. 156–159, Jan. 1970, ISSN: 0031-9007. DOI: 10.1103/PhysRevLett.24.156.

[5] Y. Huang, P. Li, R. Zhao, *et al.*, "Silica nanoparticles: Biomedical applications and toxicity," *Biomedicine & Pharmacotherapy*, vol. 151, p. 113 053, Jul. 2022, ISSN: 07533322. DOI: 10.1016/j.biopha.2022.113053.

[6] B. Jankiewicz, D. Jamiola, J. Choma, and M. Jaroniec, "Silica–metal core–shell nanostructures," *Advances in Colloid and Interface Science*, vol. 170, no. 1-2, pp. 28–47, Jan. 2012, ISSN: 00018686. DOI: 10.1016/j.cis.2011.11.002.

[7] B. Schellenberg, M. M. Behbahani, N. Balasubramanian, T. H. Fikkers, and S. Hoekstra, "Mass and shape determination of optically levitated nanoparticles," *Applied Physics Letters*, vol. 123, no. 11, Sep. 2023, ISSN: 0003-6951. DOI: 10.1063/5.0166136.

[8] K. Ullah and H. Ullah, "Enhanced optomechanically induced transparency and slow/-fast light in a position-dependent mass optomechanics," *The European Physical Journal D*, vol. 74, no. 10, p. 197, Oct. 2020, ISSN: 1434-6060. DOI: 10.1140/epjd/e2020-10286-1.

[9] R. Paschotta, "Resonator Modes - an encyclopedia article," in *RP Photonics Encyclopedia*, RP Photonics AG, 2005. DOI: 10.61835/0qg.

[10] J. C. Maxwell, "A Treatise on Electricity and Magnetism," Tech. Rep., 1873.

[11] R. Paschotta, "Gaussian Beams - an encyclopedia article," in *RP Photonics Encyclopedia*, RP Photonics AG, 2005. DOI: 10.61835/mla.

[12] J. Jahng, J. Brocious, D. A. Fishman, *et al.*, "Gradient and scattering forces in photoinduced force microscopy," *Physical Review B*, vol. 90, no. 15, p. 155 417, Oct. 2014, ISSN: 1098-0121. DOI: `10.1103/PhysRevB.90.155417`.

[13] K. C. Neuman and S. M. Block, "Optical trapping," *Review of Scientific Instruments*, vol. 75, no. 9, pp. 2787–2809, Sep. 2004, ISSN: 0034-6748. DOI: `10.1063/1.1785844`.

[14] C. F. Bohren and D. R. Huffman, *Absorption and scattering of light by small particles.* Wiley-VCH, 2009, p. 700, ISBN: 0471293407.

[15] R. D. Van Zee and J. P. Looney, *Cavity-enhanced spectroscopies.* Academic Press, 2002, p. 323, ISBN: 0124759874.

[16] E. Black, "Laser Interferometer Gravitational-Wave Observatory-LIGO-Notes on the Pound-Drever-Hall technique," Tech. Rep., 1998.

[17] E. D. Black, "An introduction to Pound–Drever–Hall laser frequency stabilization," *American Journal of Physics*, vol. 69, no. 1, pp. 79–87, Jan. 2001, ISSN: 0002-9505. DOI: `10.1119/1.1286663`.

[18] T. W. Hansch and B. Couillaud, "Of a Reflecting Reference Cavity *," Tech. Rep., 1980.

[19] G. C. Bjorklund, M. D. Levenson, W. Lenth, and C. Ortiz, "Applied physics Physics B and Laser Frequency Modulation (FM) Spectroscopy Theory of Lineshapes and Signal-to-Noise Analysis," Tech. Rep., 1983, pp. 145–152.

[20] S. Wang, W. Rong, L. Wang, H. Xie, L. Sun, and J. K. Mills, "A survey of piezoelectric actuators with long working stroke in recent years: Classifications, principles, connections and distinctions," *Mechanical Systems and Signal Processing*, vol. 123, pp. 591–605, May 2019, ISSN: 08883270. DOI: `10.1016/j.ymssp.2019.01.033`.

[21] S.-T. Ho and S.-J. Jan, "A piezoelectric motor for precision positioning applications," *Precision Engineering*, vol. 43, pp. 285–293, Jan. 2016, ISSN: 01416359. DOI: `10.1016/j.precisioneng.2015.08.007`.